Materials Science in Semiconductor Processing 107 (2020) 104863

Contents lists available at ScienceDirect

Materials Science in Semiconductor Processing

journal homepage: http://www.elsevier.com/locate/mssp

Mechanisms behind slow photoresponse character of Pulsed Electron Deposited ZnO thin films

Mehmet Özdoğan [a,b], Cem Çelebi [b], Gökhan Utlu [a,*]

[a] Department of Physics, Faculty of Science, Ege University, 35100, Izmir, Turkey
[b] Quantum Device Laboratory, Department of Physics, Izmir Institute of Technology, 35430, Izmir, Turkey

ARTICLE INFO

Keywords:
ZnO thin films
Photoresponse
Ultraviolet photodetector
Encapsulation
Defect states
Adsorbates

ABSTRACT

Semiconducting Zinc Oxide (ZnO) is ideal candidate for ultraviolet (UV) photodetector due to its promising optoelectronic properties. Photoconductive type ZnO photodetectors, which is fabricated in metal-semiconductor-metal configuration, show mostly very high photoconductivity under UV light, but they are plagued by slow photoresponse time as slow as several tens of hours, even more. Most of the studies claimed that atmospheric adsorbates such as water and oxygen create charge traps states on the surface and remarkably increase both the photoconductivity and response time. There are also limited studies, which claim that the defect states acting as hole trap centers prolong response time significantly. However, the underlying physical mechanism is still unclear. Here we study the effects of both adsorbates and defect-related states on the photoresponse character of Pulsed Electron Deposited ZnO thin films. In order to distinguish between these two mechanisms, we have compared the time-dependent photoresponse measurements of bare-ZnO and SiO_2 encapsulated-ZnO thin film samples taken under UV light and high vacuum. We show that the dominant mechanism of photoresponse in ZnO is the adsorption/desorption of oxygen and water molecules even when the measurement is performed in high vacuum. After the encapsulation of sample surface by a thin SiO_2 layer, the adsorption/desorption rates can significantly improve, and the effects of these molecules partially removed.

1. Introduction

Zinc Oxide (ZnO) material has received considerable attention due to its direct and wide bandgap (3.37 eV at room temp.) as well as large free-exciton binding energy (60 meV) for optoelectronic applications such as ultraviolet (UV) light detection for a long time [1,2]. Numerous studies have been conducted to achieve realization of electrically stable nano-electronic and nano-optoelectronic devices based on ZnO that are expected to operate a long time with reduced noise levels under atmospheric conditions; however, the electrical and optoelectronic properties of ZnO material are often changed over time [3,4]. Nanostructured or thin film forms of ZnO material are highly sensitive to environment because of their surface defects serving adsorption sites for atmospheric gases on the surface [5], which can be utilized sensitive gas detection performance [6]. Reactive gases like O_2 and H_2O in ambient can act as electron trap centers when they are stuck on the surface of n-type materials such as ZnO. Unintentional adsorption/desorption of these molecules can randomly modify the electronic transport characteristics of these kinds of materials [7–10]. The electrical conductivity of n-type ZnO material decreases upon the adsorption of these gas molecules since the main charge carriers (electrons) are captured, or increases upon desorption of these molecules from the surface [11,12]. It has been shown that the adsorbates like O_2 and H_2O can significantly change the carrier density of ZnO and strongly dominate the photoresponse characteristics of UV sensitive metal-semiconductor-metal (MSM) photoconductors fabricated out of ZnO thin films or other forms [13]. Therefore, it is of great importance to unveil the detailed physical mechanism underlying adsorbate induced electrical changes prior to designing solid-state devices out of ZnO n-type semiconductor.

In ZnO MSM photoconductors, high photoconductivity and slow photoresponsivity characters under UV light have been simultaneously observed not only due to their high sensitivity to atmosphere [14] but also their intrinsic defects acting as hole trap centers within the bandgap that prolong their response time [15]. Most of the studies suggested that the slow photoresponse character of ZnO arises from atmospheric adsorbates such as oxygen and water molecules that create charge trap states on the surface. In these studies, Ahn et al. [16] proposed that the slow photoresponse in sol-gel synthesized ZnO nanowires is due to the

* Corresponding author.
E-mail address: gokhan.utlu@ege.edu.tr (G. Utlu).

https://doi.org/10.1016/j.mssp.2019.104863
Received 27 July 2019; Received in revised form 30 October 2019; Accepted 22 November 2019
Available online 27 November 2019
1369-8001/

charge transfer between water molecules and ZnO nanowire, Soci et al. [7] obtained very high photoconductive gain as high as $G \sim 10^8$ for ZnO nanowire by means of desorption of oxygen, and Li et al. [11] proposed that the reason is due to the both effects of oxygen and water molecules. On the other hand, there are also limited studies, which claim that the reason is due to defective states behaving hole trap centers leading to significantly prolonged response time(s). For instance, Moazzami et al. [15] reported that the photoresponse of ZnO epilayers was dominated by shallow and deep trap states. However, the cause of high, but slow photoresponse character of ZnO cannot be explained via only adsorption/desorption of atmospheric species (O_2 and/or H_2O) or defect-induced states within the bandgap. It should be due to combination of both effects. In previous work [17], we have shown that in high vacuum, the photoresponse was higher and slower than that in air, confirming the atmospheric adsorbates such as O_2 and H_2O greatly dominate the photoresponsivity. And, they completely suppress the effect of defect states. In this work, therefore, we have developed an experimental approach to distinguish the effect of defect-states acting as hole trap centers from the effect of atmospheric adsorbates by simply encapsulation of ZnO thin film surface with a thin SiO_2 layer. We show that encapsulation of ZnO thin films with SiO_2 partially removes the contribution of adsorbates to photoresponse with a substantial reduction of adsorption and desorption times.

The objective of this work is to explain the aforementioned mechanisms more comprehensively and systematically, thus this study contributes to a better understanding of the ambient and intrinsic defects effects on the slow photoresponse character of ZnO nanostructures than previously reported works, and helps guide the design of ZnO-based photoconductors or gas sensors. Additionally, many encapsulation approaches have been employed for 2D materials such as HfO_2 [18] and PMMA [19] for MoS_2, SiO_2 for graphene [20]; yet, there is no detailed study investigating encapsulation effect on the photoresponse properties of ZnO thin film.

2. Experimental details

Before the deposition of ZnO thin films, Cr (3 nm)/Au (80 nm) source/drain electrodes were patterned on 10 mm × 10 mm fused-quartz substrates by thermal evaporation technique, and Fig. 1(c) shows a typical device schematic. The channel length between source and drain electrodes was set to 200 μm, and this configuration was used to Transient Photocurrent Spectroscopy (TPS) measurements. Employing a shadow mask, ~185 nm thick ZnO films with a size of 4 mm × 4 mm were deposited at the center of the substrates by state-of-the-art Pulsed Electron Deposition (PED) method. The details of PED technique can be found in Ref. [21]. The deposition parameters were fine-tuned to achieve the best ablation and plume (i.e., plasma and evaporated material) intensity, and to get high crystal quality of ZnO films. The deposition of ZnO thin films were done with a substrate temperature of 400 °C, an oxygen pressure of 1.57 Pa, an electron discharge voltage of 15 kV, and a pulse frequency of 5 Hz. Then, on the top of ZnO thin film, a thin layer of SiO_2 (~200 nm thick and 5 mm × 5 mm sized) was deposited using PED system as an encapsulation layer to assure full coverage of surface. For comparison, a set of bare ZnO thin films were also deposited by using the same protocols mentioned above.

After the successful fabrication of ZnO thin films, the structural, electrical, and opto-electronic properties of samples have been evaluated by different characterization techniques. Scanning Electron Microscopy (SEM) was performed using Carl Zeiss 300VP instrument with typically operated at 3.0 kV to characterize the ZnO thin film morphology.

The XPS analyses were performed using a Thermo Scientific Model K-Alpha XPS instrument with monochromatic Al Kα radiation (1486.68 eV) under operating pressure set to 2×10^{-7} Pa. The survey spectrum scan was completed by taking the average of 10 scans with X-ray spot size at 300 μm and passing energy at 30 eV. All the XPS spectra were calibrated by taking the C 1 s peak located at ~284 eV as a reference. Data were analyzed using Avantage XPS software package. Peak fitting

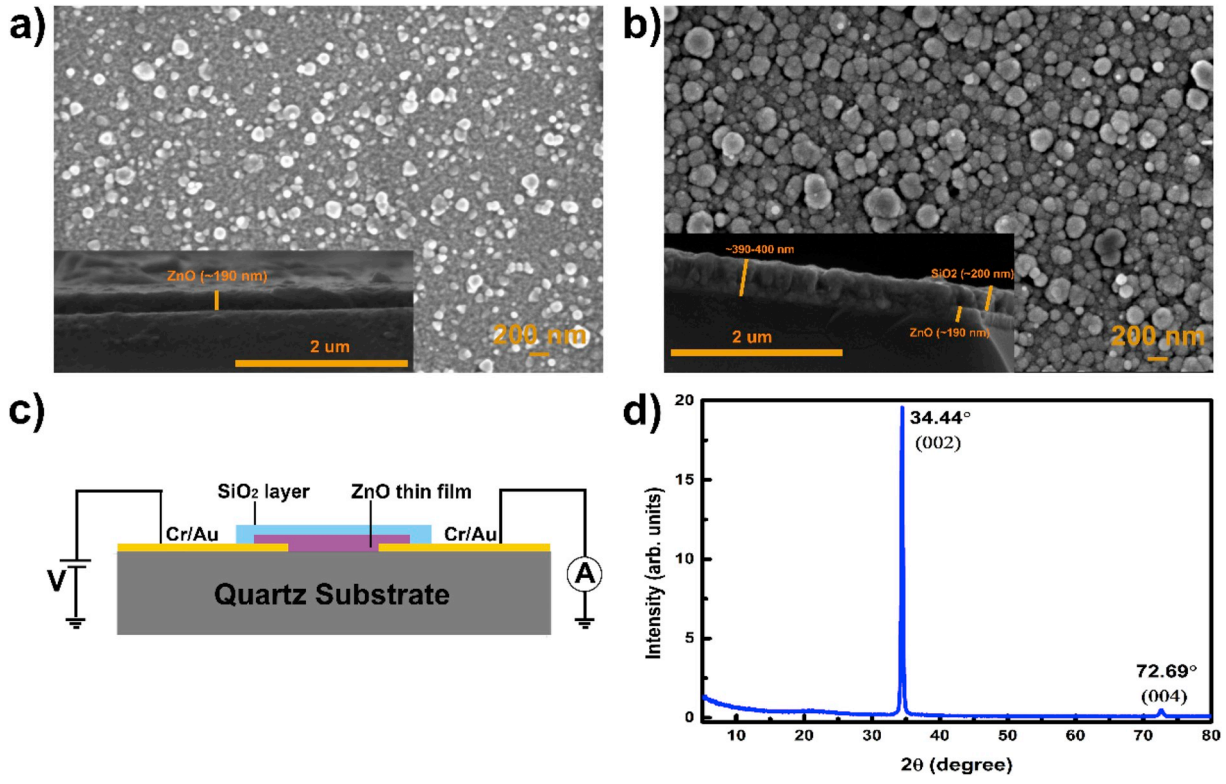

Fig. 1. SEM image of **(a)** B–ZnO and **(b)** E-ZnO samples. The insets show the related cross-sectional SEM images. **(c)** The typical device schematic of SiO_2 encapsulated-ZnO device. **(d)** XRD pattern of bare ZnO-thin film. (double-columns).

was done using Shirley/Smart type background and Gaussian/Lorentzian convolution shapes.

The X-ray diffraction (XRD) was carried out via a Philips X'Pert Pro Theta/2Theta Diffractometer with a copper K-Alpha X-ray source (λ = 1.540 Å). The scans were performed from 5° to 80° in 0.001° steps.

The Photoluminescence (PL) spectra of the samples were taken by a PerkinElmer LS-55 Luminescence Spectrometer (with a pulsed Xenon lamp) at an excitation wavelength of 350 nm with both 10 nm excitation and emission slit widths at room temperature. The excitation energy of 3.57 eV (350 nm) was slightly above the ~3.26 eV typical bandgap of our PED-fabricated samples.

Electrical and optoelectronic characterizations of the samples were done under a 254 nm wavelength UV light with an output power of 3 mW inside a high vacuum chamber with a base pressure of about 4×10^{-3} Pa. For TPS experiments, an electronic shutter mechanism was coupled to the UV light source. The photocurrent data of the samples were acquired by using Keithley 6485 Picoammeter, and Keithley 2400 Source Meter. During measurement, the applied voltage between source and drain was kept constant at 0.5 V. Prior to the each set of measurements, we conducted I–V measurements for both bare and encapsulated ZnO thin films (denoted as B–ZnO and E-ZnO, respectively) before and after TPS measurements, and then the samples were left overnight under ambient conditions in order to return back to their initial states. Afterwards, the samples were exposed to UV light for about 3 h in high vacuum to remove existing adsorbates from the surface. Right after 3 h of continuous UV light illumination, TPS measurements were conducted for short periods as 30 s with three on/off cycles to reveal time dependent photoresponse characteristics of the samples. In addition, to check the effectiveness of SiO_2 encapsulation method, we also performed same measurements for E-ZnO sample in air atmosphere.

3. Results

The SEM image of B–ZnO thin film exhibits nanoparticles appearing as white spots on the film surface as seen in Fig. 1(a). These particles are more likely to occur as a result of thin film fabrication with high energy deposition techniques such as Pulsed Laser Deposition (PLD) and PED [22,23]. However, the origin of such nanoparticles is a matter of discussion. They can be directly emitted from target during ablation process, or they can be occurred in the gas phase, during transfer of species from the target toward the substrate [24]. In addition, we conducted EDX analysis to identify the elemental compositions of these nanoparticles, and results showed that they possess almost same compositions of other regions on the film surface. The presence of such particles on the film surface increases the surface area-to-volume ratio, which maximizes the interaction between surface and atmospheric gases, and makes it more sensitive to the environment. On the other hand, Fig. 1(b) shows the E-ZnO thin film sample. When two SEM images compared, it is clear that the nanoparticles were covered by adjacent flower bud-shaped structures, confirming the successful SiO_2 encapsulation process and full coverage of surface. The insets of Fig. 1(a) and (b) show cross-sectional SEM images of B–ZnO and E-ZnO thin films, respectively. These images verify the successful deposition of each thin layer and thickness values that were measured by profilometry. Additionally, when the inset of Fig. 1(b) is examined in detail, c-axis orientation of ZnO crystallites can be seen as confirmed by XRD.

Fig. 1(d) displays the XRD pattern of B–ZnO thin film. As seen in XRD graph, the PED-fabricated ZnO thin films have a single sharp peak at an angle of around 34.44° and very small peak around 72.69° which were identified as (002) and (004) orientations of hexagonal wurtzite ZnO crystal structure. It indicates that the ZnO thin film was preferentially deposited along a c-axis orientation of the quartz substrate. This c-axis orientation of crystallites is classically observed for ZnO films, whatever the method of deposition and the substrate nature [21]. The average crystallite size (D) of ZnO thin films was calculated using the (002) major diffraction peak by Debye-Sherrer formula ($D = 089\lambda/\beta cos\theta$), and it was found to be 30.62 nm with a FWHM of 0.2716° by integrating this peak. This value is comparable to that of PLD-fabricated ZnO thin films [25].

XPS analysis was performed to get information about the surface-adsorbed species and surface chemical states of the PED-fabricated ZnO thin films. In XPS survey spectra, no elements besides Zn, O and C were detected. Fig. 2(a) shows the high-resolution XPS spectra of O1s core level. In order to further examination, the O1s peak was deconvoluted by fitting with three Gaussian/Lorentzian peaks. The deconvoluted peaks are located at binding energies 530.1, 531.0 and 532.2 eV. Here, the lower energy peak is attributed to lattice oxygen in hexagonal wurtzite structure of ZnO [26–28]. The middle peak at binding energy of 531.0 eV is associated with oxygen vacancy in ZnO lattice, corroborating the existence of surface defects on ZnO thin film. The higher energy peak corresponds to chemisorbed oxygen species such as OH^-, H_2O and O_2 [5,29,30].

The PL measurements were performed using a pulsed Xenon lamp with an excitation wavelength of 350 nm at room temperature to unveil the defect states in the PED-fabricated ZnO thin films, and Fig. 2(b) shows the PL spectrum. The raw PL data (shown in the inset of Fig. 2(b)) were processed using baseline subtraction and 2nd order Savitzky-Golay smoothing, and it was deconvoluted by fitting nine Gaussian peaks to

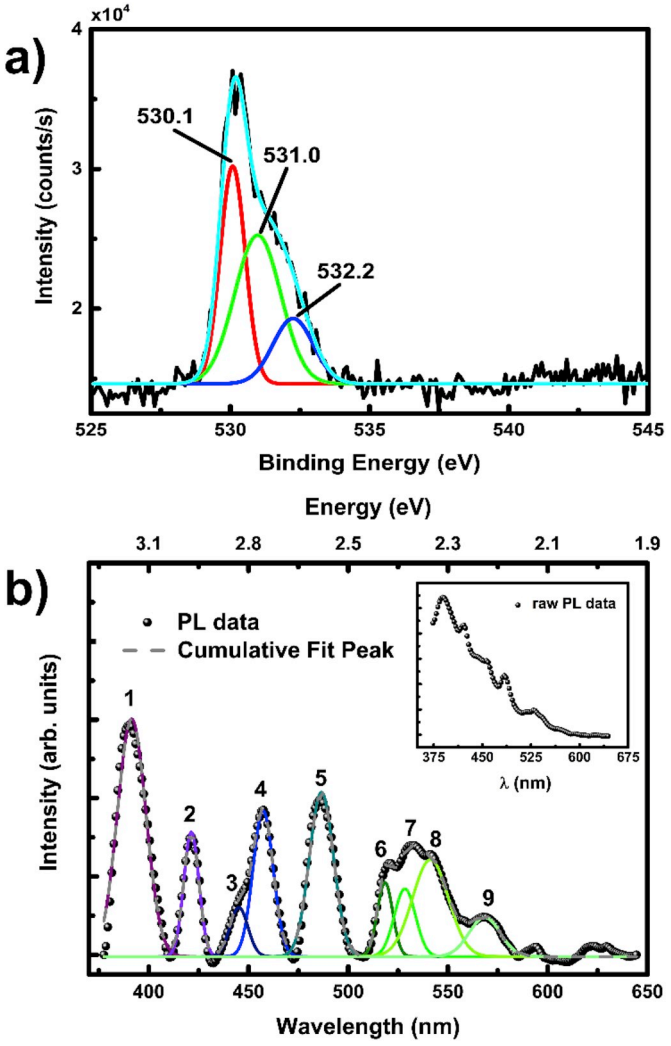

Fig. 2. (a) The high-resolution XPS chemical binding spectra O 1 s state and its deconvoluted peaks.**(b)** PL spectrum of B–ZnO thin film. In here, black circles correspond to the smoothed and baseline subtracted PL data. The numbers correspond to the deconvoluted peaks. Inset shows the raw PL spectrum. (single-column).

reveal hidden peaks. As seen in Fig. 2(b), the PL graph shows near-band emission at an energy of 3.17 eV (391.4 nm). Besides the near-band emission, the PED-fabricated ZnO thin films show emissions in the visible spectrum region 2.94–2.18 eV consisting of several distinct peaks at 2.94 eV (421.4 nm), 2.79 eV (445.2 nm), 2.71 eV (457.3 nm), 2.55 eV (486.6 nm), 2.39 eV (518.5 nm), 2.35 eV (528.4 nm), 2.29 eV (541.3 nm), and 2.18 eV (568.4 nm), indicating our ZnO thin films possess shallow states as well as deep trap states. Basically, transition from valence band (VB) to conduction band (CB), and VB to shallow defect states occurs upon photo-excitation in the PL measurement, which give rise to subsequent emissions; from CB to deep states, shallow states to VB, shallow states to deep states, and hole capture at deep states gives violet, blue and green emissions according to energy levels difference [30], as seen in Fig. 2(b). Since the excitation energy (3.57 eV) was slightly above the energy bandgap of our samples (~3.26 eV reported in our previous work [17]); therefore, the electrons excited from the VB to the CB as well as shallow defect states below the CB.

Generally oxygen vacancies are considered as the origin of observed green emission in the PL spectrum. On the other hand, zinc related defects such as; zinc interstitials (neutral, single and double ionized) are responsible for blue emission. According to the previous reports [30–35], the observed emissions in PL spectrum (Fig. 2(b)) can be summarized as follows: the transitions from 1) excitonic states to VB, or zinc interstitial states to VB, 2) CB to O interstitials states, 3) double or single ionized Zn vacancy states to VB, 4) double ionized Zn interstitials states to VB, 5) single ionized Zn interstitials states to neutral Zn vacancy states, 6) single ionized O vacancy states to VB, 7) CB to neutral antisite O states, 8) CB to antisite O or interstitials O states, and 9) CB to double ionized O vacancy states. The first four peaks (2–5) are responsible for blue emission, whereas last four peaks (6–9) are responsible for green emission. The numbers correspond to those marked peaks in Fig. 2(b).

The observed possible transitions in the PL spectrum evidence that the PED-fabricated ZnO thin films possess many defects states within the bandgap which are induced by O and Zn vacancies, O and Zn interstitial atoms, and antisite O atoms. These defects states were unintentionally introduced the ZnO structure during PED ablation process.

Fig. 3 demonstrates the I–V characteristics of B–ZnO thin film device before and after UV light exposure. It was observed that the I–V curves were perfectly linear and symmetric in both bias regions (forward and reverse), indicating good ohmic contact nature. This means that the device, which was fabricated as MSM structure, operates as photoconductor. Photoconductive type devices exhibit high dark current due to electrons are able to circulate through a circuit many times before

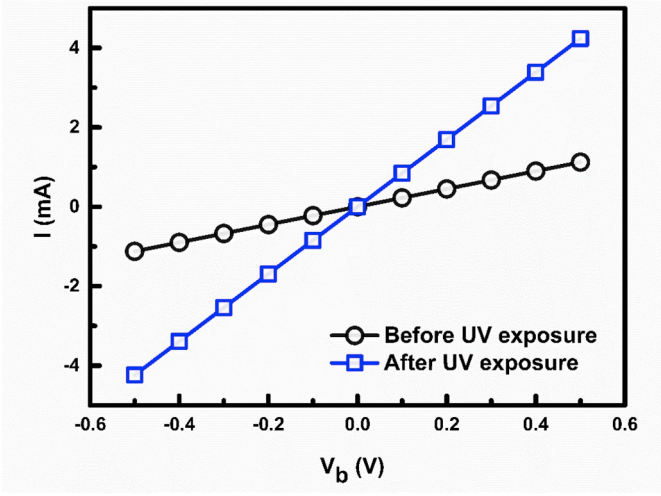

Fig. 3. I–V measurements of B–ZnO sample before and after 3 h of UV light exposure. The current data were acquired by sweeping voltage in 0.2 V steps. (single-column).

they recombine with the holes, which meanwhile remain trapped in the n-type semiconductor [36,37]. In our case and/or most of photoconductive type devices fabricated out of ZnO material, defect states in the forbidden gap result in trapping of most of holes, where stay a long time or remained trapped especially in deep trap states. Therefore, it leads to high dark current and high photoconductive gain. In addition, the adsorption/desorption of adsorbates on the surface contribute to this process by capturing/releasing electrons. The initial resistance of ZnO thin film was determined from the slope of I–V curve as 0.45 kΩ. After 3 h of UV light illumination under high vacuum, the resistance of ZnO thin film reduced to 0.12 kΩ. The observed drop in the resistance can be explained as in the following manner. The atmospheric molecules such as O_2 and H_2O are readily adsorbed onto surface of sample after exposure to air. These adsorbates behave electron trapping surface states, and hence reduce the electron density of n-type ZnO material. As the UV illumination causes desorption of these adsorbates from the sample surface into vacuum, the trapped electrons are released back to the conduction. Therefore, the resistance of the UV-illuminated sample becomes lower than that of as-grown ZnO thin film.

Now we turn to time-dependent photoresponse measurements. All measurements were done in a high vacuum (low 10^{-3} Pa) to ensure a controllable environment. During these measurements, the applied voltage between source and drain was kept constant at 0.5 V. To promote desorption of adsorbates which were already adsorbed on the surface in air, the samples were exposed to UV light. The UV irradiation wavelength was specifically selected to be 254 nm (~4.9 eV) since it is energetically sufficient enough to remove chemisorbed O_2 and H_2O molecules on the surface [38] as well as for generating electron-hole pairs in the depletion regions of ZnO thin film (E_g ~3.26 eV [17]). Time-dependent current variation of B–ZnO thin film photoconductor was shown in Fig. 4(a). The variation in the measured current $\Delta I/I_0$ (%) were determined by using the following expression;

$$\left(\frac{\Delta I}{I_0}\right) \times 100\% = \left(\frac{I - I_0}{I_0}\right) \times 100\% \quad (1)$$

where I_0 is the dark current read before UV exposure and I is the measured current after UV exposure. Upon the UV light exposure the photoresponse of sample initially increased rapidly, and a subsequent slower exponential growth was observed. After the UV light source was turned off, fast and slow exponential decay trends were observed similarly to the exponential growing parts. After 5 ks of UV illumination, the time necessary to reach a stable high vacuum condition in vacuum probe station, the variation in current of B–ZnO sample (Fig. 4(a)) was measured as high as ~380%, while for E-ZnO sample (Fig. 4(b)) was measured as ~80% according to initial values of current before the UV illumination. After the switching off the UV light, the current variation decreased to 280% according to initial level of B–ZnO, and the reduction in current measured at only one percent for E-ZnO after 10 ks time. The latter indicates the encapsulation effect on the photoresponse character. After 10 ks time interval, the current variation didn't decrease initial level (dark level) of B–ZnO sample since the oxygen and water molecules desorbed by the UV light were pumped away, and thus, the concentration of adsorbate molecules re-adsorbed on the surface is smaller than it was prior to illumination. For the case of E-ZnO, the current remained almost same during the UV light was off state, validating the effective encapsulation of surface via blocking re-adsorption of these molecules on the surface.

As mentioned above, the photoresponse characteristics of ZnO exhibit an exponential raise and decay behaviors determined by the UV light is turned on-off for B–ZnO sample. The photoresponse raised exponentially upon UV light exposure was fitted by the sum of two-exponential growth functions;

$$I = I_0 + A_1\left(1 - \exp\left(-t/\tau_f\right)\right) + A_2\left(1 - \exp\left(-t/\tau_s\right)\right) \quad (2)$$

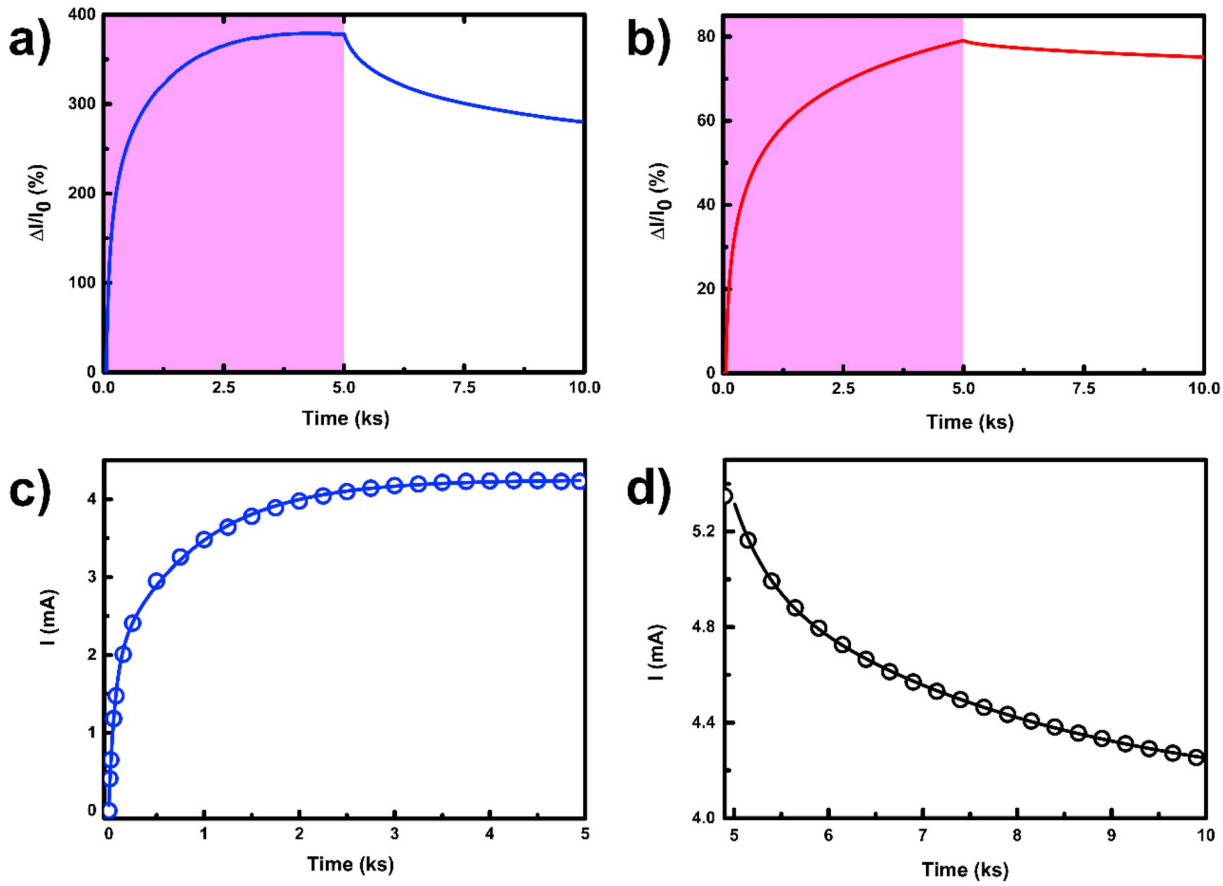

Fig. 4. The change in the currents of **(a)** B–ZnO thin film and **(b)** E-ZnO thin film samples that were exposed to 254 nm UV light for a period of 5 ks under high vacuum. After a period of 5 ks, the UV light was turned off and the samples were let to relax in high vacuum for another 5 ks The violet regions show the time interval when the UV light is on. $\Delta I = I - I_0(mA)$, where I_0 denotes the current read before UV illumination and I is the current after UV illumination. During measurement, the applied voltage between source and drain was kept constant at 0.5 V. The growing part of photoresponse variation of **(a)** B–ZnO thin film was shown in **(c)** with blue circles, while the decaying part was shown in **(d)** with black circles. Blue and red curves illustrate the fitted curves using Eqs. (2) and (3), respectively. (double-columns).

and it was shown in Fig. 4(c) with a blue line. In equation (2), the A_1 and A_2 fit constants, I_0 correspond to related dark current read before the illumination, $I_0 = 4.27\ mA$(ohmic contact leads to high dark current), and the extracted time constants were $\tau_f = 0.09$ ks and $\tau_s = 0.97$ ks corresponding to the first and second terms of Eq. (2), respectively. Here τ_f is the time constant of fast component and τ_s is the time constant of slow component. When turning the UV light off, the observed decrease in photoresponse was fitted by the sum of two-exponential decay functions as;

$$I = I_0 + A_1 exp\left(-t/\tau_f\right) + A_2 exp\left(-t/\tau_s\right) \quad (3)$$

where $I_0 = 4.06\ mA$, and the extracted time constants are $\tau_f = 0.36$ ks and $\tau_s = 3.14$ ks corresponding to the first and second terms in Eq. (3), respectively. The fitted curve was shown in Fig. 4(d) with a black line.

In our previous work [17], we have compared the photoresponse properties of PED-fabricated ZnO thin film for air and high vacuum environments, and we saw that the photoresponse decreases faster in air (with a ~%45 relative humidity) and reaches initial condition upon turning the light off, indicating water adsorption leads to quick restore of current. The reason is that when the water molecules are adsorbed with the hydrogen sides on the surface, which are positively charged due to the high electronegativity of oxygen than hydrogen [16], they capture more electrons than oxygen. In addition, Li et al. [11] reported that water adsorption especially at high humidity cases (>70%) leads to the fast shortening of the photocurrent in decaying stage for ZnO nanowires. Moreover, Panda et al. [39] reported two time constants for current decaying stage of thermally grown ZnO thin films, and they related the fast decay time to water adsorption, the slow decay rate to oxygen adsorption. According to our results and literature, we concluded that the estimated two fast time constants in above are more likely to occur with photo-assisted desorption/adsorption of H_2O molecules from the surface, whereas the slow time constants are due to relatively slow desorption/adsorption rate of O_2 molecules from the surface.

As seen in Fig. 4(a), the growing and decaying part of photoresponse variation are not symmetric. Decaying part of current does not decrease to the initial level due to reduced concentration of adsorbate molecules in the stable high vacuum. This clearly shows the effect of atmospheric adsorbates on the photoresponse characteristics of our samples. In the decaying part, the fast time constant is 4 times as large relative to fast time constant for growing part (0.36 ks/0.09 ks corresponding to re-adsorption of H_2O, whereas the slow time constant is ~3.2 times higher than that of the growing part (3.14 ks/0.97 ks as a consequence of re-adsorption of O_2 molecules on the surface. When the high vacuum reached its stable value (~5.0×10^{-3} Pa), the desorbed H_2O and O_2 molecules from the surface with the help of UV light were mostly evacuated from the environment. Therefore, fast and slow time constants were largely increased since re-adsorption rates were greatly decreased due to lack of adsorbate molecules, and consequently an asymmetric trend was observed in the photoresponse character determined by the UV light was turned on-off. This indicates that the dominant mechanism of photoresponse in ZnO is adsorption/desorption of atmospheric species on the surface, and it is difficult to distinguish

photo-generation/recombination times from these relatively large time constants. Therefore, to eliminate adsorbate effects on the photo-response, we have encapsulated the surface of ZnO with a thin layer of SiO_2.

In Fig. 5, we have compared the photoresponse behaviors of B–ZnO and E-ZnO thin films by taking short periods TPS measurements. The TPS measurements were conducted for short periods as 30 s with three on/off cycles. Prior to the these measurements, both samples were exposed to UV light in high vacuum for duration of ~3 h to make sure that all possible adsorbates were removed greatly from surfaces. To quantitatively examine the results, short-period TPS curves were fitted using the same two-component exponential functions presented above in Eqs. (2) and (3), and thus the time constants were extracted. For the experiments, we first started to short period TPS measurements with UV light was on state, and after 30 s time interval, the shutter was closed (off state). In Fig. 5(a), following a very small but sharp drop within 3.2 s, an exponential decay trend in the measured current was observed as a consequence of the re-adsorption of a trace amount of adsorbates on the sample surfaces with an adsorption time of 74.8 s. When turning the UV light on, a very small increment occurred due to the contribution of photo-generated charge carriers within ~2.0 s, which was followed by an exponential increment in the current due to photo-desorption process with a desorption time of 35.4 s. The adsorption rate with the estimated time constant ($\tau_{ad} = 74.8$ s) was found to be smaller than desorption rate ($\tau_{des} = 35.4$ s) of B–ZnO sample. The drastic difference between the adsorption and desorption rates leads to a downward trend in the overall current variation within a couple of on/off cycles as seen in Fig. 5(a). On the other hand, after the SiO_2 encapsulation of ZnO surface, the sharp drop time decreased to 0.8 s as turning the UV light off, and the adsorption rate was estimated as 30.6 s. When turning the UV light on, photo-generation occurred within a 0.7 s, which was followed by an exponential increment with a desorption rate of 19.3 s, at the sensitivity limits of our measuring system. These results apparently indicate that the surface encapsulation method notably reduce the estimated time constants for both adsorption and desorption rates. Additionally, it reveals more reasonable photo-generation and recombination time constants. Besides, when the amplitudes of current variations of B–ZnO and E-ZnO samples were compared, the amplitude of E-ZnO sample was almost one order of magnitude smaller than that of bare counterpart, indicating adsorbates responsible for high photoconductivity, and after encapsulation process, the effect of adsorbate molecules were partially eliminated.

To check the effectiveness of SiO_2 encapsulation method, we conducted the short-period TPS measurements in air ambient for E-ZnO sample. As seen in Fig. 6, the results indicate that SiO_2 encapsulation approach is still valid for the blocking of surface interactions with atmosphere.

The photoresponse properties of ZnO thin films greatly improved after the encapsulation of surface with a thin layer of SiO_2. The TPS plots of E-ZnO thin film exhibit an almost symmetric trend in both environments; high vacuum and air. Once the UV light is turned off, the photocurrent of the E-ZnO sample decreased to its initial level indicating enhanced stability and reversibility of our device. Despite the encapsulation significantly improve the device performance, there would be another possible mechanism that still leads to exponential behavior seen in Fig. 5(b), as explained in the discussion section.

4. Discussion

Possible technological applications of ZnO materials in the fields of gas sensors and optoelectronics have been investigated for many years [40], but the relation between the material surface and atmospheric adsorbates have not been fully understood yet. In fact, its photoresponse is mainly governed by the charge transfer doping phenomenon that occur during adsorption/desorption of adsorbates in air as previously discussed [11,41]. When the adsorbates like O_2 and H_2O in air are stuck on the surface of ZnO nanostructures especially with high surface area-to-volume ratio, they trap free electrons by creating a low conductivity depletion layer in the vicinity of surface. The trapped electrons are released fast at first via desorption of H_2O molecules, and then continues at a slower rate due to desorption of O_2 molecules under UV light that promotes desorption process. As evidenced in our XPS results, the PED-fabricated ZnO thin films possess oxygen vacancies on the surface, which they serve active areas for the adsorption of O_2 and H_2O molecules. These results confirm our suggestions about adsorption/desorption mechanism in ZnO thin films with large surface area-to-volume ratios.

For ZnO thin film with inherently high surface area-to-volume ratio

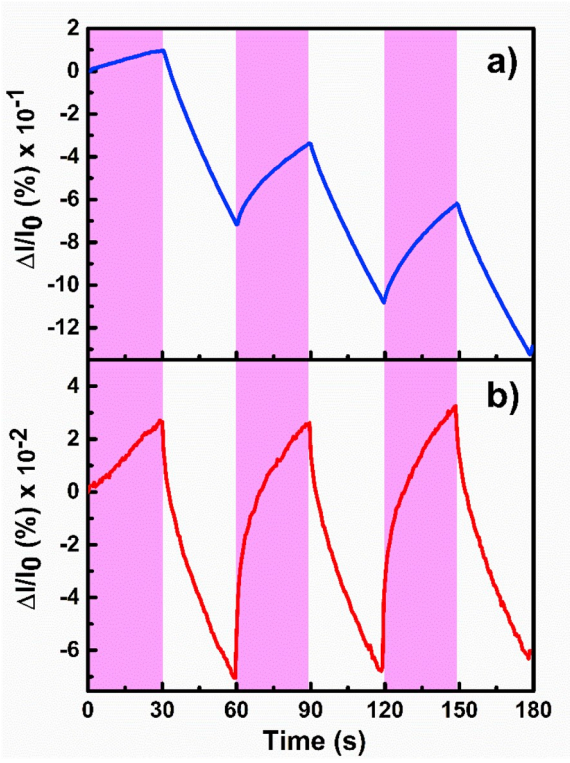

Fig. 5. Short-period TPS measurements of **(a)** B–ZnO thin film and **(b)** E-ZnO thin film. The violet regions show the time intervals when the UV light is on. During measurement, the applied voltage between source and drain was kept constant at 0.5 V. (single-column).

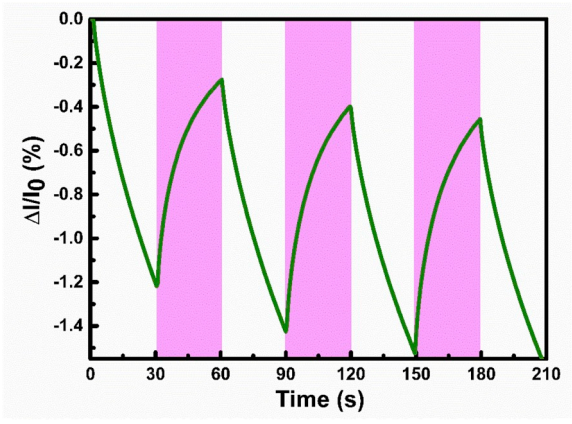

Fig. 6. Short-period TPS measurements of E-ZnO thin film in air atmosphere with relative humidity of 40–45%. The violet regions show the time intervals when the UV light is on. During measurement, the applied voltage between source and drain was kept constant at 0.5 V. (single-column).

as a result of high energy deposition technique like PED in our case, the conductivity is mainly governed by the adsorption/desorption of atmospheric adsorbates. In the light of the experimental results obtained in 5 ks photoresponse measurements (Fig. 4(a)), the conductivity changes can be written in the form of $\Delta\sigma_{ZnO}(t) \propto \sigma_{des}(t)$ under UV illumination. Here, $\sigma_{des}(t)$ is the contribution of photo-desorption of adsorbates from surfaces to conductivity. The contribution of photo-desorption process, $\sigma_{des}(t)$, can be divided into two components as $\sigma_{des}(t) = \sigma^{f}_{H_2O}(t) + \sigma^{s}_{O_2}(t)$. Here, $\sigma^{f}_{H_2O}(t)$ is the contribution of fast component by reason of water desorption, while $\sigma^{s}_{O_2}(t)$ is the contribution of slow component by reason of oxygen desorption. These fast and slow terms vary as a function of time in the form of $\sigma^{f}_{H_2O}(t) = 1 - e^{-t/\tau_f}$ and $\sigma^{s}_{O_2}(t) = 1 - e^{-t/\tau_s}$ corresponding to the first and second terms in the right side of Eq. (2), respectively. On the other hand, upon turning the UV light off the alteration in conductivity occurred as $\Delta\sigma_{ZnO}(t) \propto -\sigma_{ad}(t)$. Here $\sigma_{ad}(t)$ is the contribution of the re-adsorption of adsorbates on the surface of film. The same two aforementioned components (fast and slow) are responsible for exponential decay of photoresponse. Therefore, fast and slow decay processes change as a function of time $\sigma^{f}_{H_2O}(t) = e^{-t/\tau_f}$ and $\sigma^{s}_{O_2}(t) = e^{-t/\tau_s}$, respectively.

To get deeper insights into the photoresponse character of ZnO thin film under UV light, we have conducted short period TPS measurements. The results reveal that the conductivity variations can be written in the form of $\Delta\sigma_{B-ZnO}(t) \propto \sigma_{ph} + \sigma_{des}(t)$ under UV exposure, σ_{ph} is the contribution of photo-induced charge carriers in the depletion layers of ZnO thin film. When the UV light is turned off, the conductivity changes can be written as $\Delta\sigma_{B-ZnO}(t) \propto -(\sigma_{ph} + \sigma_{des}(t))$. The observed exponential trend proves the $\sigma_{ph} \ll \sigma_{des}(t)$ due to surface layers that absorb most of UV photons for desorption process.

In this work, we showed an experimental method that inhibits the interactions between atmosphere and surface simply by a SiO_2 encapsulation layer. Therefore, we assumed that the contribution of adsorbates to the photoresponse character was completely blocked by means of encapsulation. However, despite the effect of adsorbates on the photocurrent variation was inhibited, the exponential trend was still observed in Fig. 5(b). As known in literature, the existence of intrinsic defects in the crystal structure would introduce several defect states acting as hole trap centers within the bandgap of any semiconductor [15,42,43]. Our PL and XPS results confirm the existence of many defective states both on the surface and within the bandgap of PED-fabricated ZnO thin films. Therefore, even if we isolate the surface of ZnO thin film from the environment, the photo-generated holes are mostly trapped at these defect states leaving behind unpaired electrons in the ZnO that still contribute to the photocurrent. Due to the lifetime of these unpaired electrons is further increased by trapped holes; the recombination rate of electron-hole pairs is progressively slowing down. The additional contribution of trap-states to the conductivity (σ_{trap}) plays another role on the overall conductivity variation of ZnO thin film ($\Delta\sigma \propto \sigma_{ph} + \sigma_{trap}$) determined by the UV light is on-off. Eventually, ZnO thin film shows slow photoresponse to UV light leading to exponential behavior as still seen in Fig. 5(b).

5. Conclusion

In summary, we investigated the mechanisms behind slow photoresponse behavior of the PED-fabricated ZnO thin films. The slow photoresponse of ZnO occurs because of two mechanisms acting simultaneously, which make it difficult to pick out the individual mechanism since the effect of adsorbates is dominant. To eliminate the effect of adsorbate, we encapsulated the surface of ZnO with a thin layer of SiO_2. We see that defect-induced hole trap-states plays another role on the overall conductivity variation of ZnO thin film, which still leads to slow photoresponse to continue. Therefore, controlling intrinsic defects during material growth process as well as encapsulation process is important to obtain fast speed UV photodetector fabricated out of ZnO material.

We believe that our results lead the way for future application of high speed and sensitive ZnO photodetector with choosing effective encapsulation materials and prompt for further investigation in encapsulation of other n-type materials.

Declaration of competing interest

The authors declare that they have no known competing financial interests or personal relationships that could have appeared to influence the work reported in this paper.

Acknowledgements

The authors would like to thank Serap Yiğen for the encapsulation experiments, and S. Batuhan Kalkan for the experimental setup. Characterizations of samples were conducted in the Center for Materials Research of İzmir Institute of Technology (IYTE-MAM), Ege University Central Research Test & Analysis Laboratory Application & Research Center (EGE-MATAL) and İzmir Katip Çelebi University Central Research Lab. A part of this work has been supported by Ege University Scientific Research Project (BAP) with Project No. 15-FEN-058.

References

[1] Ü. Özgür, Y.I. Alivov, C. Liu, A. Teke, M.A. Reshchikov, S. Doğan, V. Avrutin, S.-J. Cho, H. Morkoç, A comprehensive review of ZnO materials and devices, J. Appl. Phys. 98 (2005) 041301, https://doi.org/10.1063/1.1992666.

[2] A. Janotti, C.G. Van de Walle, Fundamentals of zinc oxide as a semiconductor, Rep. Prog. Phys. 72 (2009) 126501, https://doi.org/10.1088/0034-4885/72/12/126501.

[3] M. Ghosh, R.S. Ningthoujam, R.K. Vatsa, D. Das, V. Nataraju, S.C. Gadkari, S. K. Gupta, D. Bahadur, Role of ambient air on photoluminescence and electrical conductivity of assembly of ZnO nanoparticles, J. Appl. Phys. 110 (2011) 054309, https://doi.org/10.1063/1.3632059.

[4] B. Claflin, D.C. Look, D.R. Norton, Changes in electrical characteristics of ZnO thin films due to environmental factors, J. Electron. Mater. 36 (2007) 442–445, https://doi.org/10.1007/s11664-006-0063-7.

[5] V. Bhatt, M. Kumar, J. Kim, H.-J. Chung, J.-H. Yun, Persistent photoconductivity in Al-doped ZnO photoconductors under air, nitrogen and oxygen ambiance: role of oxygen vacancies induced DX centers, Ceram. Int. 45 (2019) 8561–8570, https://doi.org/10.1016/j.ceramint.2019.01.174.

[6] L. Zhu, W. Zeng, Room-temperature gas sensing of ZnO-based gas sensor: a review, Sens. Actuators A Phys. 267 (2017) 242–261, https://doi.org/10.1016/j.sna.2017.10.021.

[7] C. Soci, A. Zhang, B. Xiang, S.A. Dayeh, D.P.R. Aplin, J. Park, X.Y. Bao, Y.H. Lo, D. Wang, ZnO nanowire UV photodetectors with high internal gain, Nano Lett. 7 (2007) 1003–1009, https://doi.org/10.1021/nl070111x.

[8] P. Han, E.R. Adler, Y. Liu, L. St Marie, A. El Fatimy, S. Melis, E. Van Keuren, P. Barbara, Ambient effects on photogating in MoS 2 photodetectors, Nanotechnology 30 (2019) 284004, https://doi.org/10.1088/1361-6528/ab149e.

[9] H.-C. Chang, Y.-J. Huang, H.-Y. Chang, W.-J. Su, Y.-T. Shih, Y.-S. Huang, K.-Y. Lee, Oxygen adsorption effect on nitrogen-doped graphene electrical properties, Appl. Phys. Express 7 (2014) 055101, https://doi.org/10.7567/APEX.7.055101.

[10] J.-H. Ahn, W.M. Parkin, C.H. Naylor, A.T.C. Johnson, M. Drndić, Ambient effects on electrical characteristics of CVD-grown monolayer MoS2 field-effect transistors, Sci. Rep. 7 (2017) 4075, https://doi.org/10.1038/s41598-017-04350-z.

[11] Y. Li, F. Della Valle, M. Simonnet, I. Yamada, J.-J. Delaunay, Competitive surface effects of oxygen and water on UV photoresponse of ZnO nanowires, Appl. Phys. Lett. 94 (2009) 023110, https://doi.org/10.1063/1.3073042.

[12] Y. Jin, J. Wang, B. Sun, J.C. Blakesley, N.C. Greenham, Solution-processed ultraviolet photodetectors based on colloidal ZnO nanoparticles, Nano Lett. 8 (2008) 1649–1653, https://doi.org/10.1021/nl0803702.

[13] J. Zhou, Y. Gu, Y. Hu, W. Mai, P.-H. Yeh, G. Bao, A.K. Sood, D.L. Polla, Z.L. Wang, Gigantic enhancement in response and reset time of ZnO UV nanosensor by utilizing Schottky contact and surface functionalization, Appl. Phys. Lett. 94 (2009) 191103, https://doi.org/10.1063/1.3133358.

[14] Q.H. Li, T. Gao, Y.G. Wang, T.H. Wang, Adsorption and desorption of oxygen probed from ZnO nanowire films by photocurrent measurements, Appl. Phys. Lett. 86 (2005) 123117, https://doi.org/10.1063/1.1883711.

[15] K. Moazzami, T.E. Murphy, J.D. Phillips, M.C.K. Cheung, A.N. Cartwright, Sub-bandgap photoconductivity in ZnO epilayers and extraction of trap density spectra, Semicond. Sci. Technol. 21 (2006) 717–723, https://doi.org/10.1088/0268-1242/21/6/001.

[16] S.-E. Ahn, H.J. Ji, K. Kim, G.T. Kim, C.H. Bae, S.M. Park, Y.-K. Kim, J.S. Ha, Origin of the slow photoresponse in an individual sol-gel synthesized ZnO nanowire, Appl. Phys. Lett. 90 (2007) 153106, https://doi.org/10.1063/1.2721289.

[17] M. Özdoğan, S. Yiğen, C. Çelebi, G. Utlu, The comparison of transient photocurrent spectroscopy measurements of Pulsed Electron Deposited ZnO thin film for air and vacuum ambient conditions, Thin Solid Films 680 (2019) 48–54, https://doi.org/10.1016/j.tsf.2019.04.030.
[18] D. Kufer, G. Konstantatos, Highly sensitive, encapsulated MoS 2 photodetector with gate controllable gain and speed, Nano Lett. 15 (2015) 7307–7313, https://doi.org/10.1021/acs.nanolett.5b02559.
[19] W. Park, J. Park, J. Jang, H. Lee, H. Jeong, K. Cho, S. Hong, T. Lee, Oxygen environmental and passivation effects on molybdenum disulfide field effect transistors, Nanotechnology 24 (2013) 095202, https://doi.org/10.1088/0957-4484/24/9/095202.
[20] S.B. Kalkan, S. Yiğen, C. Çelebi, Epitaxial graphene thermistor for cryogenic temperatures, Sens. Actuators A Phys. 280 (2018) 8–13, https://doi.org/10.1016/j.sna.2018.07.028.
[21] S. Tricot, M. Nistor, E. Millon, C. Boulmer-Leborgne, N.B. Mandache, J. Perrière, W. Seiler, Epitaxial ZnO thin films grown by pulsed electron beam deposition, Surf. Sci. 604 (2010) 2024–2030, https://doi.org/10.1016/j.susc.2010.08.016.
[22] A. Ali, R. Henda, R. Fagerberg, Effect of temperature and discharge voltage on the properties of Co-doped ZnO thin films deposited by pulsed electron beam ablation, Appl. Surf. Sci. 422 (2017) 1082–1092, https://doi.org/10.1016/j.apsusc.2017.06.123.
[23] M. Nistor, W. Seiler, C. Hebert, E. Matei, J. Perrière, Effects of substrate and ambient gas on epitaxial growth indium oxide thin films, Appl. Surf. Sci. 307 (2014) 455–460, https://doi.org/10.1016/j.apsusc.2014.04.056.
[24] M. Nistor, N.B. Mandache, J. Perrière, Pulsed electron beam deposition of oxides thin films, J. Phys. D Appl. Phys. 41 (2008) 165205, https://doi.org/10.1088/0022-3727/41/16/165205.
[25] M. Naouar, I. Ka, M. Gaidi, H. Alawadhi, B. Bessais, M.A.E. Khakani, Growth, structural and optoelectronic properties tuning of nitrogen-doped ZnO thin films synthesized by means of reactive pulsed laser deposition, Mater. Res. Bull. 57 (2014) 47–51, https://doi.org/10.1016/j.materresbull.2014.05.020.
[26] L.-J. Meng, C.P. Moreira de Sá, M.P. dos Santos, Study of the structural properties of ZnO thin films by x-ray photoelectron spectroscopy, Appl. Surf. Sci. 78 (1994) 57–61, https://doi.org/10.1016/0169-4332(94)90031-0.
[27] P.-T. Hsieh, Y.-C. Chen, K.-S. Kao, C.-M. Wang, Luminescence mechanism of ZnO thin film investigated by XPS measurement, Appl. Phys. A 90 (2007) 317–321, https://doi.org/10.1007/s00339-007-4275-3.
[28] Y.F. Lu, H.Q. Ni, Z.H. Mai, Z.M. Ren, The effects of thermal annealing on ZnO thin films grown by pulsed laser deposition, J. Appl. Phys. 88 (2000) 498–502, https://doi.org/10.1063/1.373685.
[29] M. Chen, X. Wang, Y. Yu, Z. Pei, X. Bai, C. Sun, R. Huang, L. Wen, X-ray photoelectron spectroscopy and auger electron spectroscopy studies of Al-doped ZnO films, Appl. Surf. Sci. 158 (2000) 134–140, https://doi.org/10.1016/S0169-4332(99)00601-7.
[30] R. Khokhra, B. Bharti, H.-N. Lee, R. Kumar, Visible and UV photo-detection in ZnO nanostructured thin films via simple tuning of solution method, Sci. Rep. 7 (2017) 15032, https://doi.org/10.1038/s41598-017-15125-x.
[31] S. Mandal, M.L.N. Goswami, K. Das, A. Dhar, S.K. Ray, Temperature dependent photoluminescence characteristics of nanocrystalline ZnO films grown by sol–gel technique, Thin Solid Films 516 (2008) 8702–8706, https://doi.org/10.1016/j.tsf.2008.05.016.
[32] K. Lim, M. Abdul Hamid, R. Shamsudin, N.H. Al-Hardan, I. Mansor, W. Chiu, Temperature-driven structural and morphological evolution of zinc oxide nano-coalesced microstructures and its defect-related photoluminescence properties, Materials (Basel) 9 (2016) 300, https://doi.org/10.3390/ma9040300.
[33] C.H. Ahn, Y.Y. Kim, D.C. Kim, S.K. Mohanta, H.K. Cho, A comparative analysis of deep level emission in ZnO layers deposited by various methods, J. Appl. Phys. 105 (2009) 013502, https://doi.org/10.1063/1.3054175.
[34] K. Bandopadhyay, J. Mitra, Zn interstitials and O vacancies responsible for n-type ZnO: what do the emission spectra reveal? RSC Adv. 5 (2015) 23540–23547, https://doi.org/10.1039/C5RA00355E.
[35] K. Vanheusden, W.L. Warren, C.H. Seager, D.R. Tallant, J.A. Voigt, B.E. Gnade, Mechanisms behind green photoluminescence in ZnO phosphor powders, J. Appl. Phys. 79 (1996) 7983–7990, https://doi.org/10.1063/1.362349.
[36] G. Konstantatos, E.H. Sargent, Nanostructured materials for photon detection, Nat. Nanotechnol. 5 (2010) 391–400, https://doi.org/10.1038/nnano.2010.78.
[37] F.H.L. Koppens, T. Mueller, P. Avouris, A.C. Ferrari, M.S. Vitiello, M. Polini, Photodetectors based on graphene, other two-dimensional materials and hybrid systems, Nat. Nanotechnol. 9 (2014) 780–793, https://doi.org/10.1038/nnano.2014.215.
[38] S.B. Kalkan, H. Aydın, D. Özkendir, C. Çelebi, The effect of adsorbates on the electrical stability of graphene studied by transient photocurrent spectroscopy, Appl. Phys. Lett. 112 (2018) 013103, https://doi.org/10.1063/1.5011454.
[39] S.K. Panda, C. Jacob, Preparation of transparent ZnO thin films and their application in UV sensor devices, Solid State Electron. 73 (2012) 44–50, https://doi.org/10.1016/j.sse.2012.03.004.
[40] K. Liu, M. Sakurai, M. Aono, ZnO-based ultraviolet photodetectors, Sensors 10 (2010) 8604–8634, https://doi.org/10.3390/s100908604.
[41] K. Keem, H. Kim, G.-T. Kim, J.S. Lee, B. Min, K. Cho, M.-Y. Sung, S. Kim, Photocurrent in ZnO nanowires grown from Au electrodes, Appl. Phys. Lett. 84 (2004) 4376–4378, https://doi.org/10.1063/1.1756205.
[42] J. Jiang, C. Ling, T. Xu, W. Wang, X. Niu, A. Zafar, Z. Yan, X. Wang, Y. You, L. Sun, J. Lu, J. Wang, Z. Ni, Defect engineering for modulating the trap states in 2D photoconductors, Adv. Mater. 30 (2018) 1804332, https://doi.org/10.1002/adma.201804332.
[43] W. Fei-Fei, W. Chong, C. Ke, Z. Bing-Suo, Trap induced slow photoresponse of single CdS nanoribbons, Chin. Phys. B 17 (2008) 3103–3107, https://doi.org/10.1088/1674-1056/17/8/056.